Novel Ultrafast Spiral Head MR Angiography Compared to Standard MR and CT Angiography

Tobias Greve*, Nico Sollmann*, Andreas Hock, Claus Zimmer, and Jan S. Kirschke

From the Department of Diagnostic and Interventional Neuroradiology, Klinikum rechts der Isar, Technische Universität München, Munich, Germany (TG, NS, CZ, JSK); Department of Neurosurgery, University Hospital, Ludwig-Maximilians-University, Campus Grosshadern, Munich, Germany (TG); TUM-Neuroimaging Center, Klinikum rechts der Isar, Technische Universität München, Munich, Germany (NS, CZ, JSK); and Health Systems Philips Switzerland, Horgen, Switzerland (AH).

ABSTRACT

BACKGROUND AND PURPOSE: **Intracranial vessel imaging by time-of-flight MR angiography (TOF-MRA) is one of the most frequently performed investigations in clinical neuroradiology. Particularly in the acute setting, fast imaging is needed for diagnostics, with a sequence ideally depicting even small vessels. The purpose of this study was to compare image and diagnostic quality of a novel ultrashort TOF-MRA sequence accelerated by spiral imaging (TOF-Spiral-short) to a standard TOF-MRA sequence accelerated by compressed sensing (TOF-CS) and to CT angiography (CTA).**

METHODS: **Forty-one patients (36.6% showing vessel pathologies) who had undergone TOF-CS (acquisition duration: 4 minutes 8 seconds), TOF-Spiral-short (acquisition duration: 51 seconds; spiral imaging [accelerating factor 1.3], decreased field of view [accelerating factor 1.2], and increased voxel size [accelerating factor 3.3]), and CTA were retrospectively evaluated. Assessment of image quality, diagnostic confidence, and quantification of stenosis or aneurysm diameter were performed by two readers.**

RESULTS: **Image quality at the skull base was slightly reduced with TOF-Spiral-short compared to CTA and TOF-CS ($P < .05$). Delineation of small intracranial vessels was improved by TOF-Spiral-short compared to CTA ($P < .0001$). In TOF-Spiral-short, diagnostic confidence was not reduced compared to TOF-CS in patients with vessel pathologies. We observed no significant difference in quantitative pathology assessment between TOF-Spiral-short and the other two modalities. TOF-Spiral-short enabled the correct identification of all vessel pathologies.**

CONCLUSIONS: **Accelerating TOF-MRA of brain-feeding arteries by a novel ultrashort spiral imaging sequence shows adequate image quality and sufficient diagnostic performance. Thus, TOF-Spiral-short holds potential for fast and reliable diagnostics of vessel pathologies, particularly in the acute setting.**

Keywords: Aneurysm, cerebral arteries, magnetic resonance angiography, parallel imaging, stroke.

Acceptance: Received July 16, 2020, and in revised form September 10, 2020. Accepted for publication September 14, 2020.

Correspondence: Address correspondence to Nico Sollmann, Department of Diagnostic and Interventional Neuroradiology, Klinikum rechts der Isar, Technische Universität München, Ismaninger Str. 22, 81675 Munich, Germany. E-mail: Nico.Sollmann@tum.de.

*These authors contributed equally to this work.

Acknowledgements and Disclosure: The authors of this manuscript declare relationships to Philips Healthcare, whose products and services were related to the subject matter of the article. The study was completely financed by institutional grants of the Department of Neuroradiology.
Open access funding enabled and organized by Projekt DEAL.

J Neuroimaging 2020;00:1-12.
DOI: 10.1111/jon.12791

Introduction

Fast, reliable, and safe imaging of cerebral vasculature is of utmost importance for diagnostics, treatment planning, and patient counseling in diseases that affect the intra- or extracranial brain-feeding arteries, with ischemic stroke due to thromboembolic vessel occlusion representing the entity in this spectrum with the highest morbidity and economic impact.[1–3] Digital subtraction angiography (DSA) is usually regarded as the gold-standard method in arterial intracranial vessel imaging especially in complex pathologies where high-resolution imaging is warranted, but this technique holds important limitations, namely, the necessity of applying iodinated contrast agents, exposure to radiation, restricted availability, and possible procedural complications due to the invasiveness of the approach.[4,5] CT angiography (CTA) is the standard modality when acute onset neurological deficits warrant rapid imaging of the brain-feeding arteries.[6] However, vessel evaluation can be impaired in calcified atherosclerotic vasculature.[6–8] Furthermore, CTA also employs iodinated contrast agents and radiation, thereby limiting its usage or at least requiring careful evaluation of indication.[9]

Time-of-flight MR angiography (TOF-MRA) is based on a 3-dimensional multiple volume acquisition for an optimal inflow effect and has evolved as an important alternative imaging modality, rendering intravenous contrast agents and exposure to radiation unnecessary.[10–13] However, the technique is comparatively slow, and generating a spatial resolution below 1 millimeter with an acceptable signal-to-noise ratio (SNR) within an acceptable scan time can be challenging and is commonly achieved by limiting the field of view (FOV).[14] Different techniques to accelerate TOF-MRA have evolved over the recent years, one of which is compressed sensing, an undersampling

algorithm of the k-space that is increasingly used in various MRI applications.[15–21]

Spiral imaging is another method that has recently been introduced to clinical imaging applications. TOF-MRA using spiral imaging, as employed in this study, utilizes a stack of spirals with an in-plane spiral-out trajectory that has the advantage of short echo times (TEs) and an intrinsic compensation for higher gradient moments.[22,23] Blurring due to off-resonance is usually corrected during reconstruction based on a magnetic field map acquired prior to the spiral scan.[24] Studies have shown the usability of spiral imaging in T1-weighted spin echo sequences.[25] Recently, it has been demonstrated that spiral imaging can be used to generate TOF-MRA sequences in a comparable amount of time when compared to TOF-MRA accelerated by compressed sensing.[26]

Due to the inherent advantages of spiral imaging mentioned above, we hypothesize that it can markedly accelerate TOF-MRA, thereby outperforming other acceleration algorithms such as TOF-MRA accelerated by compressed sensing, with only minor drawbacks regarding coverage, spatial resolution, or diagnostic quality. For this purpose, we qualitatively and quantitatively compared a newly implemented ultrashort and optimized TOF-MRA sequence using spiral imaging to our hospital-intern standard TOF-MRA sequence employing compressed sensing and the gold-standard method of CTA.

Methods

Ethics

This retrospective single-center study was approved by the local institutional review board of our hospital (registration number: 1/19 S). Informed consent was waived due to the retrospective design of the study.

Study Setup and Purpose

In December 2018 and January 2019, 119 patients with indication for MRI-based imaging of brain-feeding arteries underwent TOF-MRA, employing one Compressed SENSE (CS) sequence (TOF-CS; acquisition duration: 4 minutes 8 seconds) and one ultrashort sequence using spiral imaging (TOF-Spiral-short; acquisition duration: 51 seconds). Acquisition of these sequences took place in the context of the 8-week initiation phase of a new MRI scanner software being capable of applying spiral imaging. Patients who underwent TOF-MRA in this initiation phase were retrospectively identified in our hospital's institutional digital Picture Archiving and Communication System (PACS).

For this study, the following inclusion criteria were defined: (1) age above 18 years, (2) referral for MRI with an indication for imaging of brain-feeding arteries, (3) acquisition of two TOF-MRA sequences: TOF-CS and TOF-Spiral-short, and (4) previous or later acquisition of CTA of brain-feeding arteries as the gold-standard method (maximum interval of 1 week between TOF-MRA and CTA). Furthermore, the following exclusion criteria were determined: (1) motion artifacts in CTA and/or TOF-MRA imaging data to a degree hampering unequivocal evaluation of vessel walls or pathology (10 patients; 6 patients with motion artifacts in both TOF-CS and TOF-Spiral-short and 4 patients with motion artifacts in TOF-CS only), (2) artifacts in CTA and/or TOF-MRA imaging data due to foreign objects, and (3) revascularization of a previously occluded vessel or stenting, clipping, or coiling performed during the interval between CTA and TOF-MRA imaging (in patient cases with thromboembolic vessel occlusion, stenosis, or aneurysms).

Table 1. Acquisition Parameters of Time-of-Flight Magnetic Resonance Angiography

Sequence	TOF-CS	TOF-Spiral-short
Acquisition type	3-dimensional	3-dimensional
TR/TE (ms)	25/3.5	25/3.5
Min TE (ms)	3.1	1.31
TE characteristics	Out-phase, 3.45 ms	Out-phase, 3.45 ms
Acquired voxel size (mm)	0.8 × 0.7 × 0.4	1.1 × 0.82 × 0.82
Field of view (mm)	200 × 200 × 88	200 × 200 × 70
Flip angle (degree)	20	20
Partial echo	Yes	No
CS factor	5	–
Denoising	Strong	–
Readout duration (ms)	–	10
Spiral interleaves	–	22
Acquisition duration	4 minutes 8 seconds	51 seconds

CS = Compressed SENSE; TE = echo time; TOF = time-of-flight; TR = repetition time.

The final diagnosis of vessel pathology during clinical routine was based on CTA and our conventionally acquired TOF-CS sequence in combination with previous or later DSA examinations, if performed, thus considering all available imaging data. In this study, the TOF-Spiral-short sequence is systematically compared to CTA and to TOF-CS as our institution's internal reference sequence for MRI-based imaging of brain-feeding arteries.

Imaging of Brain-Feeding Arteries

Computed Tomography Angiography

The CTA data used in this study were derived from scanning on a multidetector CT (MDCT) scanner (Ingenuity Core 128, Philips Healthcare, Best, The Netherlands). Standard bolus triggering was used during CTA acquisition, with the region of interest (ROI) being located in the descending aorta. The examinations were performed after administration of intravenous contrast agent (Iomeprol, Imeron 400, Bracco Imaging, Milano, Italy), with injections being administered at a flow rate of 4 mL/seconds (total volume of contrast agent of 50 mL, followed by injection of 10 mL of saline solution). The acquisition started with a delay of 6 seconds after mean attenuation in the ROI reached 120 Hounsfield Units. The tube voltage was 120 kVp, and the tube current was implicitly modulated by the scanner software during the gantry's rotation. CTA data were reconstructed using iterative reconstruction as provided by the MDCT system.

Magnetic Resonance Angiography

All TOF-MRA imaging was performed on the same 3-Tesla MRI scanner (Achieva dStream, Philips Healthcare) using product software R5.6, enabling CS and spiral imaging. Scanning was performed head first in supine position using a 32-channel head coil.

The TOF-CS and TOF-Spiral-short sequences were acquired as part of multisequence imaging protocols that were

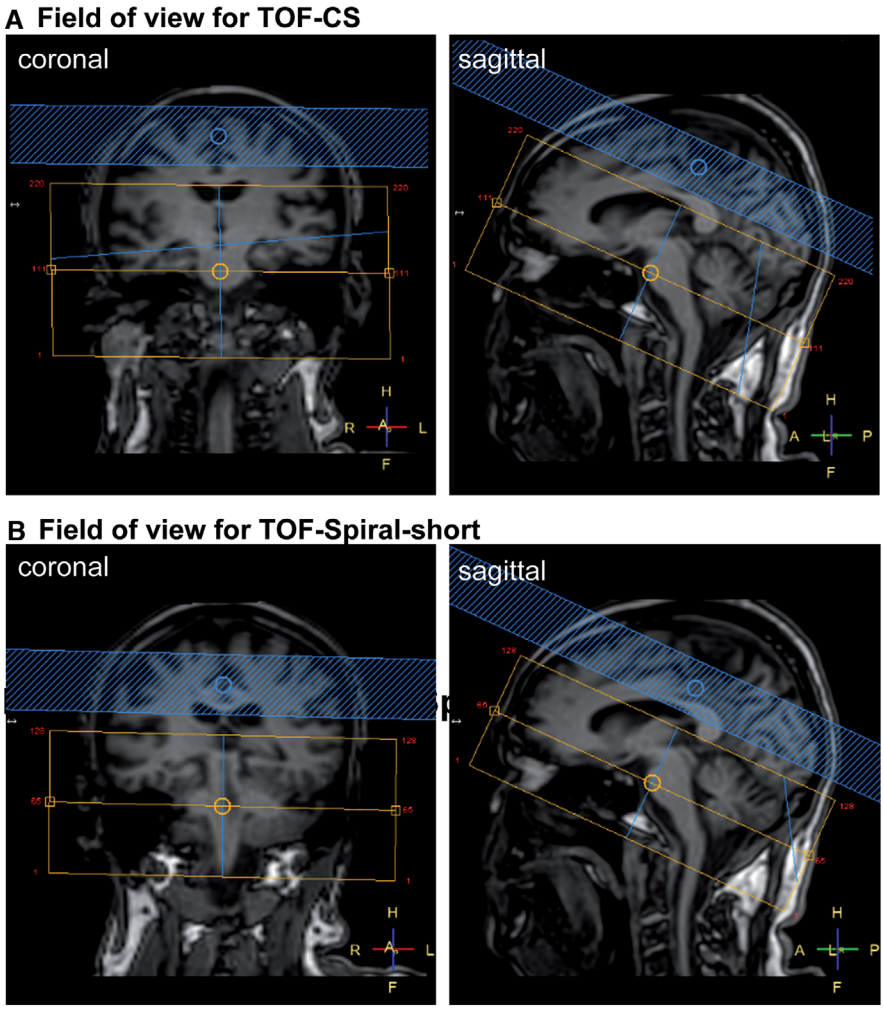

Fig 1. Female patient with vertigo and ataxia undergoing MRI including time-of-flight MR angiography (TOF-MRA) to rule out ischemia of the brain stem. The planning of the field of view (FOV) is depicted for the TOF-MRA sequence acquired with Compressed SENSE (TOF-CS; A) and spiral imaging (TOF-Spiral-short; B). The FOV of TOF-Spiral-short was reduced in its craniocaudal dimensions to further decrease acquisition time.

individually adapted according to the clinical indication. Because TOF-CS is the dedicated MRA technique in our institution in clinical practice, it was acquired first in all patients, whereas TOF-Spiral-short was acquired subsequently. In case that contrast agent was applied, the TOF-CS and TOF-Spiral-short sequences were acquired prior to administration by default. Relevant acquisition parameters of the sequences are displayed in Table 1. A 3-dimensonal magnetic field map to correct for off-resonance was acquired in the first 10 seconds of the TOF-Spiral-short (included in the acquisition time of 51 seconds for the TOF-Spiral-short sequence).

Acquisition planning was identical for both TOF-MRA sequences and was performed in an individual survey scan. The FOV was manually centered on the supposed location of the Circle of Willis, and the plane between the foramen magnum and nasion was chosen as a reference for determining the angulation. The exact size of the FOV was predetermined for both TOF-MRA sequences and was the same in all enrolled patients. Specifically, the FOV of TOF-CS was 18 mm larger in craniocaudal dimensions and the voxel size of TOF-Spiral-short was .52 mm^3 larger compared to TOF-CS (Table 1). TOF-Spiral-short was faster than TOF-CS by a factor of ~5. This was achieved by (1) spiral imaging, accelerating by a factor of 1.3, (2) decreased FOV, accelerating by a factor of 1.2, and (3) increased voxel size, accelerating by a factor of 3.3.

Despite the smaller FOV in TOF-Spiral-short, each sequence's FOV allowed for depiction of at least the distal extracranial, intraosseous, and intradural internal carotid artery (ICA), the anterior cerebral artery (ACA; A1 and A2 segments), middle cerebral artery (MCA; M1 to M3 segments), posterior cerebral artery (PCA; P1 to P2 segments), distal vertebral artery (VA), and basilar artery (BA). A saturation band was placed above the FOV and the auto-shim function was applied (Fig 1). Furthermore, two reconstruction samples were deposited for both TOF-MRA sequences, respectively, generating maximum intensity projections (MIPs) with left-right and up-down rotations.

Evaluation of Imaging Data

Evaluation of CTA and TOF-MRA imaging data was independently performed by two readers (two neuroradiologists with 7 and 4 years of experience in neuroradiological imaging, reader 1 [R1] and reader 2 [R2]). Both qualitative and quantitative

Table 2. Scoring System for Qualitative Image Evaluation

Image Quality: Large Vessels					
	Score				
	1	2	3	4	5
Extracranial ICA Intraosseous ICA Intradural ICA VA and BA	Evaluation of vessel occlusion not possible Unacceptable diagnostic quality	Evaluation of vessel stenosis not possible Unacceptable diagnostic quality	Evaluation of vessel stenosis possible Acceptable diagnostic quality	Evaluation of vessel wall possible – only small artifacts present No compromise of diagnostic quality	No artifacts No compromise of diagnostic quality

Detectability: Medium Vessels				
	Score			
	0	1	2	3
ACA	Unclear/not distinguishable	Only A1 segment distinguishable	A1 and A2 segments distinguishable	–
MCA		Only M1 segment distinguishable	M1 and M2 segments distinguishable	M1, M2, and M3 segments distinguishable
PCA		Only P1 segment distinguishable	P1 and P2 segments distinguishable	–

Detectability: Small Vessels			
	Score		
	0	1	2
AChA	Unclear/not distinguishable	Distinguishable to level of brainstem	Distinguishable to level of ventricle (temporal horn)
SUCA		Distinguishable to level of cerebellar peduncle	Distinguishable to cerebellar parenchyma
PCOM left		Distinguishable in its entire course	–
PCOM right		Distinguishable in its entire course	–

ACA = anterior cerebral artery; AChA = anterior choroidal artery; BA = basilar artery; ICA = internal carotid artery; MCA = middle cerebral artery; PCA = posterior cerebral artery; PCOM = posterior communicating artery; SUCA = superior cerebellar artery; VA = vertebral artery.

evaluations were performed in the PACS viewer (IDS7, Sectra AB, Linköping, Sweden).

Prior to assessments, image layouts showing the CTA, TOF-CS, and TOF-Spiral-short sequences (including MIP reconstructions) were generated, with the patient and TOF-MRA sequence details hidden. Furthermore, readers were not allowed to access the reports created during clinical routine or any other imaging data of the enrolled patients. The order of image assessments for qualitative evaluations was randomized (eg, analysis started with the CTA, TOF-CS, or TOF-Spiral-short imaging data). In case that the CTA covered a larger area (eg, FOV covering at least the aortic arch to the vertex) when compared to the TOF-MRA sequences, the evaluation of CTA was restricted to the area that both CTA and TOF-MRA imaging data had in common.

Qualitative Analysis and Diagnostic Confidence

Qualitative analyses were separately performed for the CTA, TOF-CS, and TOF-Spiral-short imaging data using a standardized scoring scheme (Table 2). Similar scoring systems have been used in previous publications on evaluations of CTA or TOF-MRA images.[26,27]

Scoring included the assessment of image quality and image artifacts of large vessels (extracranial ICA, intraosseous ICA, intradural ICA, VA, and BA) and detectability of medium vessels (ACA, MCA, and PCA with their proximal to distal segments) as well as small vessels (anterior choroidal artery [AChA], superior cerebellar artery [SUCA], and posterior communicating artery [PCOM]). Except for evaluations of the PCOM (separate assessment of the left and right PCOM), scorings were based on evaluations of the vessels of both hemispheres together in case of bilateral existence. Furthermore, readers counted the number of vessel pathologies per patient, the affected vessel and segment, side, and type of abnormality, if any (stenosis, occlusion, or aneurysm).

Diagnostic confidence was determined according to a three-point grading scheme (1 = low, 2 = intermediate, and 3 = high diagnostic confidence) in each sequence. In patients without registered vessel pathologies or with only one vessel pathology,

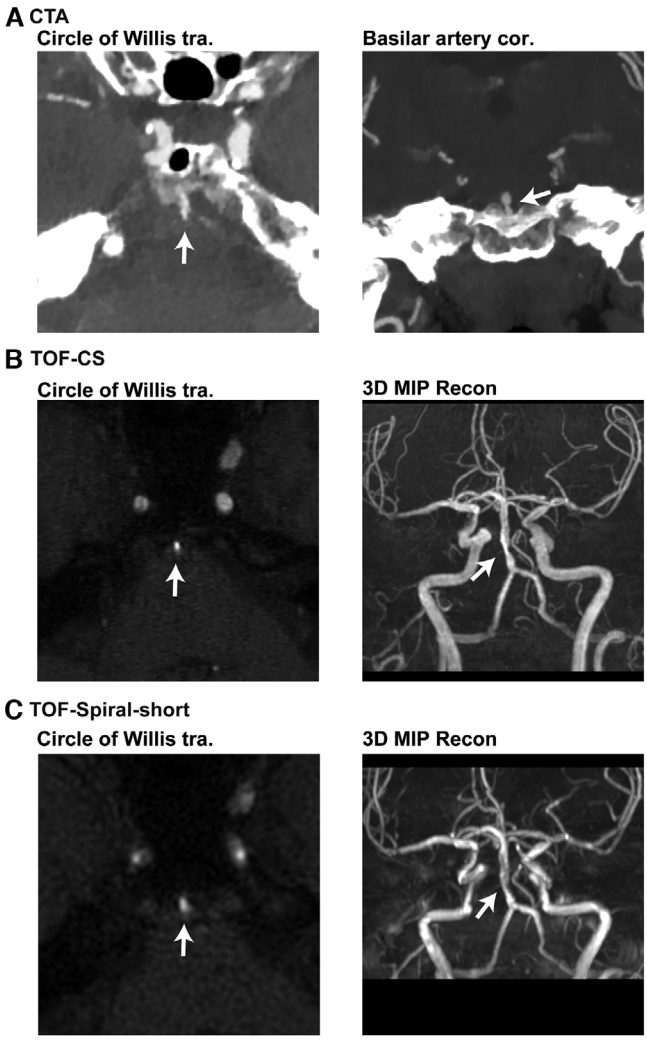

Fig 2. Male patient with painless paresis of the left lower extremity. Imaging revealed a short-path stenosis of the basilar artery (arrows) and subacute ischemia in the primary motor cortex (not shown). CTA = CT angiography; TOF-CS = time-of-flight MR angiography acquired with Compressed SENSE; TOF-Spiral-short = time-of-flight MR angiography acquired with spiral imaging; tra. = transversal; cor. = coronal; MIP = maximum intensity projection; Recon = image reconstruction.

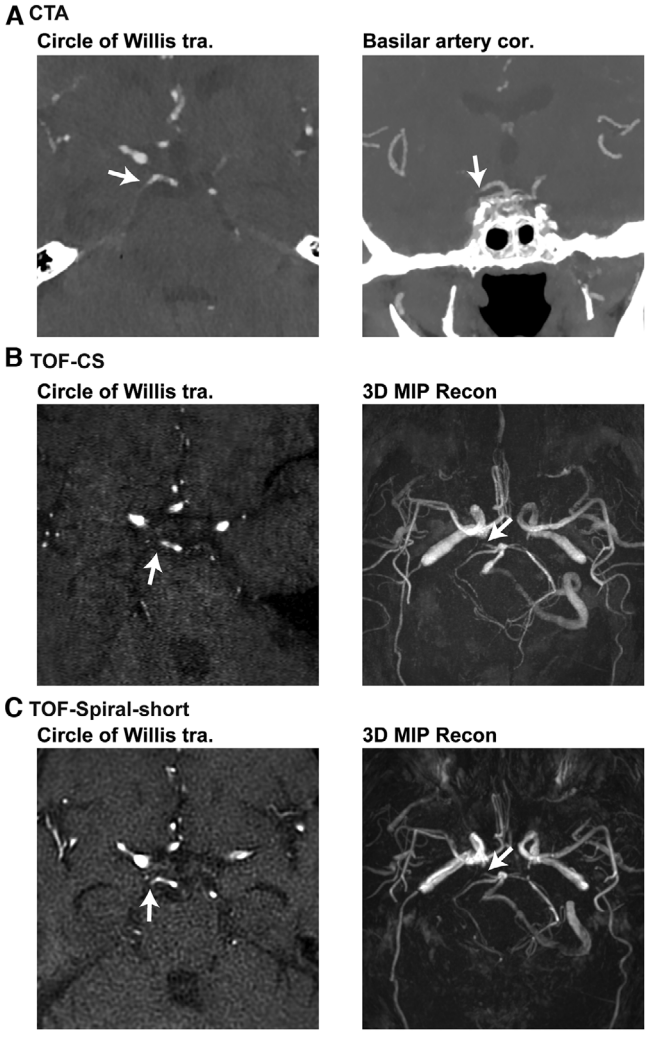

Fig 3. Male patient with sudden onset of visual field defects and a vessel occlusion at the P1/P2 junction of the right posterior cerebral artery (arrows). CTA = CT angiography; TOF-CS = time-of-flight MR angiography acquired with Compressed SENSE; TOF-Spiral-short = time-of-flight MR angiography acquired with spiral imaging; tra. = transversal; cor. = coronal; MIP = maximum intensity projection; Recon = image reconstruction.

one score for diagnostic confidence was assigned. In patients with more than one vessel pathology, one distinct score for diagnostic confidence was determined for each detected vessel pathology.

Quantitative Analysis

In patients with at least one detected vessel pathology (stenosis, occlusion, or aneurysm), quantitative analyses were performed in addition to qualitative evaluations based on the CTA, TOF-CS, and TOF-Spiral-short imaging data. All measurements were performed with standard tools implemented in the PACS viewer.

Concerning aneurysms, the maximum diameter was measured while considering all available plains. For stenoses, the North American Symptomatic Carotid Endarterectomy Trial (NASCET) criteria were considered to determine the degree of lumen stenosis for both extra- and intracranial arterial vessels.[28–30] In patients with complete vessel occlusions, no quantitative parameters were extracted from the image data. In case of more than one detected vessel pathology per patient, each pathology was measured separately.

Statistical Analysis

Statistical analysis was performed with GraphPad Prism (version 7.0; GraphPad Software Inc) and SPSS (version 26.0; IBM SPSS Statistics for Windows), with a P-value $< .05$ indicating statistical significance. Descriptive statistics were calculated for patient characteristics and demographics and, furthermore, for the scores of qualitative analyses and diagnostic confidence as well as for quantitative analyses. Scores for diagnostic confidence were analyzed separately for patients with and without vessel pathologies, and quantitative analyses were considered in patients with aneurysms and patients with stenosis, respectively.

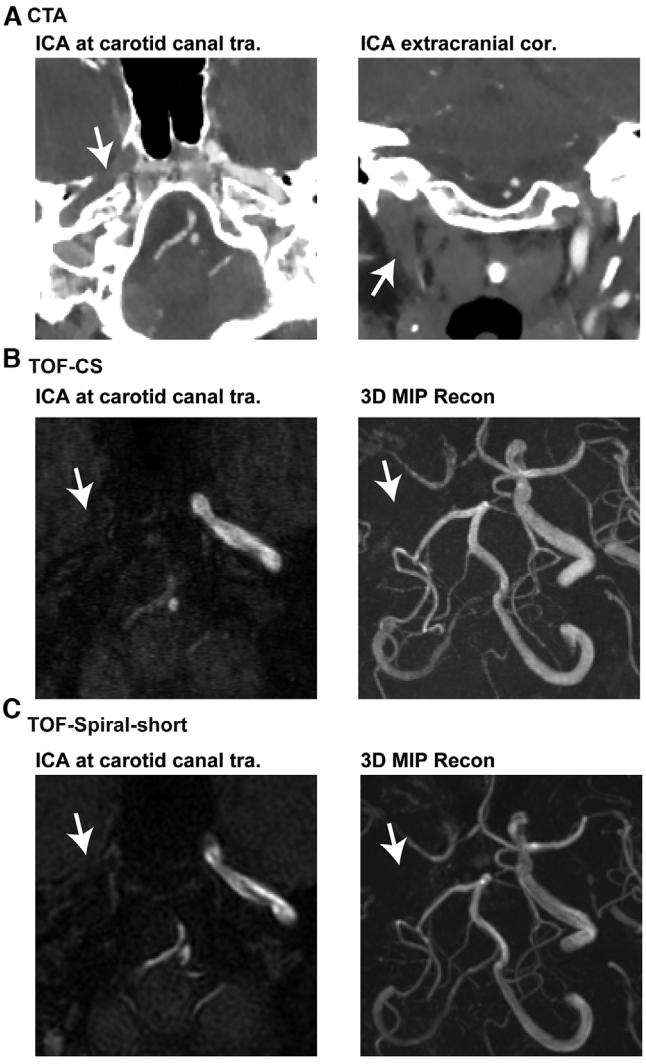

Fig 4. Male patient with transient ischemic attack (amaurosis fugax). Imaging revealed an occlusion of the internal carotid artery (ICA; arrows) at the right side without signs of acute ischemia. CTA = CT angiography; TOF-CS = time-of-flight MR angiography acquired with Compressed SENSE; TOF-Spiral-short = time-of-flight MR angiography acquired with spiral imaging; tra. = transversal; cor. = coronal; MIP = maximum intensity projection; Recon = image reconstruction.

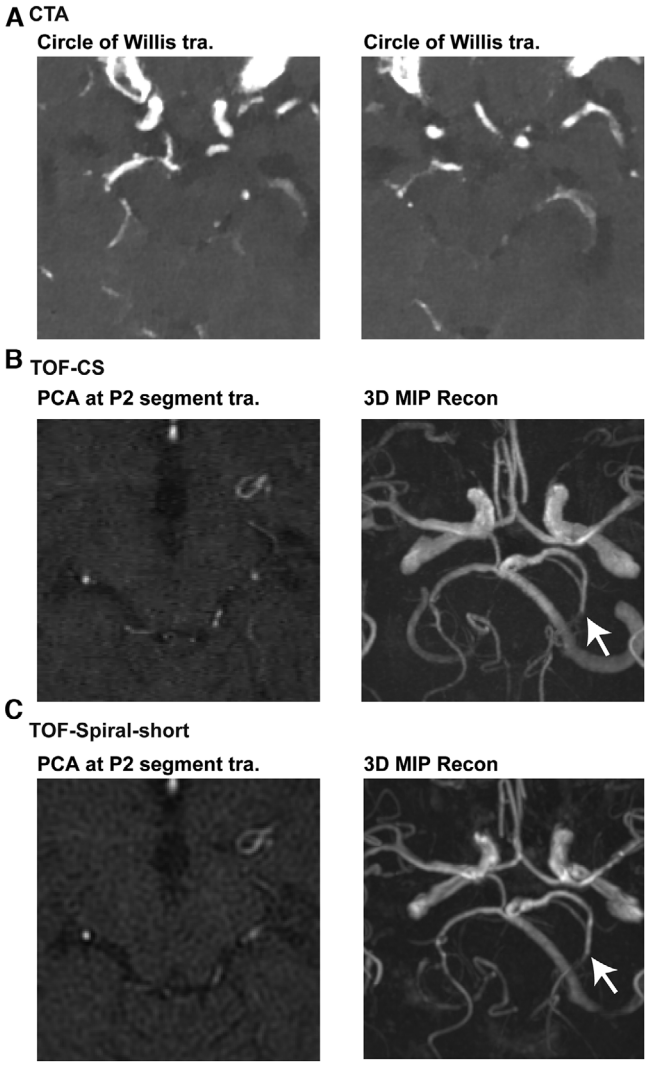

Fig 5. Female patient with sudden onset of hypesthesia. Imaging revealed a short occlusion of the P2 segment of the posterior cerebral artery (PCA; arrows) at the left side with signs of acute ischemia in the left thalamus (not shown). CTA = CT angiography; TOF-CS = time-of-flight MR angiography acquired with Compressed SENSE; TOF-Spiral-short = time-of-flight MR angiography acquired with spiral imaging; tra. = transversal; MIP = maximum intensity projection; Recon = image reconstruction.

To compare scores assigned for image quality, detectability of medium vessels, detectability of small vessels, and diagnostic confidence among evaluations of CTA, TOF-CS, and TOF-Spiral-short imaging data, Wilcoxon signed-rank tests were conducted based on the evaluations of both readers, respectively. To evaluate interreader agreement between the evaluations of R1 and R2, weighted Cohen's kappa was calculated. For measurements of maximum aneurysm diameter or degree of stenosis, Wilcoxon signed-rank tests were performed among values derived from CTA, TOF-CS, and TOF-Spiral-short imaging data, again discriminating between the evaluations of both readers. Furthermore, correlations in quantitative analyses between readers were assessed by means of the intraclass correlation coefficient (ICC). Furthermore, the rate of pathology detection was compared to the final clinical diagnosis using the combined consensus reading of CTA, TOF-CS, and DSA, if available.

Results

Study Cohort

Forty-one patients (mean age: 65.8 ± 17.9 years, age range: 18.2-93.7 years; 36.6% females) fulfilled the inclusion criteria and were enrolled in this study. The average time interval between the beginning of the MRI examination and the completion of acquisition of the TOF-CS and TOF-Spiral-short sequences was 16.1 ± 2.2 minutes (time range: 10.0-24.0 minutes).

The concluding clinical diagnosis using a combined consensus reading with CTA, TOF-CS, and DSA (if available) ruled out vessel pathologies in 26 patients (63.4%), whereas 15 patients (36.6%) showed at least one vessel pathology. Among these 15 patients, 25 vessel pathologies of different entity (stenosis, occlusion, or aneurysm) were recorded in total. In detail, 11 vessel pathologies were stenoses (44.0%; Fig 2), occlusions accounted for nine vessel pathologies (36.0%; Figs 3-5), and

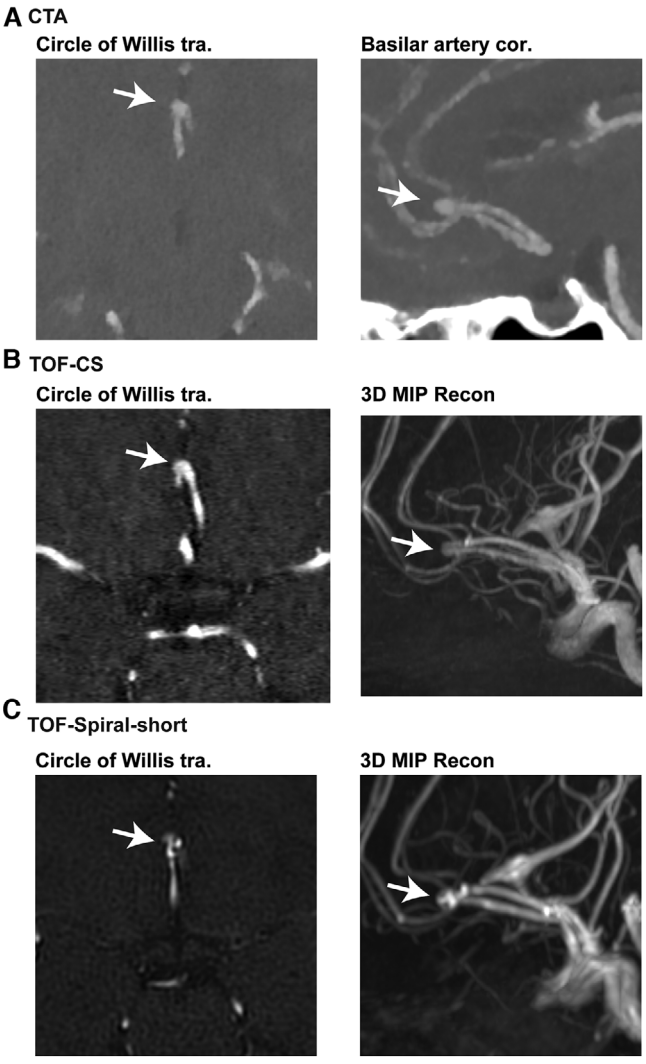

Fig 6. Female patient with sudden onset of headache and cervical neck pain. Imaging revealed an aneurysm of the anterior cerebral artery (arrows) without signs of related subarachnoid hemorrhage. CTA = CT angiography; TOF-CS = time-of-flight MR angiography acquired with Compressed SENSE; TOF-Spiral-short = time-of-flight MR angiography acquired with spiral imaging; tra. = transversal; cor. = coronal; MIP = maximum intensity projection; Recon = image reconstruction.

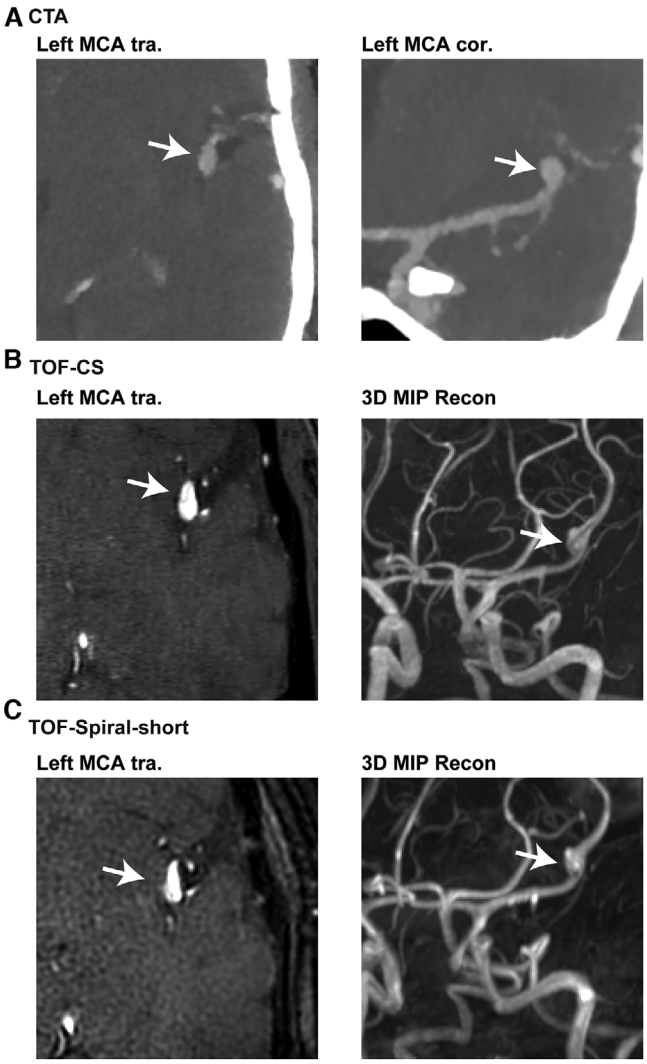

Fig 7. Female patient with sudden headache. Imaging revealed an aneurysm of the left middle cerebral artery (MCA; arrows) without signs of related subarachnoid hemorrhage. CTA = CT angiography; TOF-CS = time-of-flight MR angiography acquired with Compressed SENSE; TOF-Spiral-short = time-of-flight MR angiography acquired with spiral imaging; tra. = transversal; cor. = coronal; MIP = maximum intensity projection; Recon = image reconstruction.

aneurysms were noted for the remaining five vessel pathologies (20.0%; Figs 6 and 7). These vessel pathologies affected the ICA (28.0%), M1 segment (20.0%) or M2 segment (12.0%), BA (12.0%) or V4 segment (12.0%), P1 segment (8.0%) or P2 segment (4.0%), and A2 segment (4.0%).

Qualitative Analysis

Table 3 shows the results for large vessel image quality and medium and small vessel detectability. Worse scores were assigned in TOF-Spiral-short when compared to CTA or TOF-CS for large vessel image quality ($P < .05$); however, the image quality for VA, BA, and extracranial ICA was still high with only minor image artifacts. A more prominent drawback was found for TOF-Spiral-short at the intradural and intraosseous ICA, where image quality was only rated as acceptable (Fig 8).

Regarding detectability of the ACA, MCA, and PCA and their segments, differences were not detectable when comparing CTA or TOF-CS to TOF-Spiral-short imaging data ($P > .05$). Detectability of small vessels such as the AChA or SUCA was better in TOF-Spiral-short sequences when compared to CTA imaging data ($P < .0001$), whereas differences were not detectable between the left- and right-sided PCOM ($P > .05$; Fig 8).

Diagnostic Confidence

Table 4 displays the results for diagnostic confidence. In patients without suspected vessel pathologies, average diagnostic confidence was high for CTA, TOF-CS, and TOF-Spiral-short imaging data (except for the evaluation of R2 for the TOF-Spiral-short imaging data, which was of intermediate diagnostic confidence). Similarly, diagnostic confidence was also intermediate to high in patients with vessel pathologies, with no significant differences between scores assigned in CTA or TOF-CS compared to TOF-Spiral-short ($P > .05$). Interreader

Table 3. Large Vessel Image Quality and Medium and Small Vessel Detectability

Vessel/Segment	Reader	CTA	TOF-CS	TOF-Spiral-short	*p* (CTA vs. TOF-Spiral-short)	*p* (TOF-CS vs. TOF-Spiral-short)
Extracranial ICA	R1	4.8 ± .4	4.8 ± .4	3.8 ± .5	<.0001	<.0001
	R2	4.6 ± .5	4.8 ± .5	3.8 ± .7	<.0001	<.0001
Intraosseous ICA	R1	4.5 ± .6	4.6 ± .5	3.0 ± .7	<.0001	<.0001
	R2	4.4 ± .7	4.8 ± .4	3.1 ± .8	<.0001	<.0001
Intradural ICA	R1	4.4 ± .7	4.2 ± .7	3.1 ± .7	<.0001	<.0001
	R2	4.4 ± .7	4.3 ± .7	3.2 ± .8	<.0001	<.0001
VA and BA	R1	4.3 ± .7	4.1 ± .8	3.6 ± .7	<.0001	.0003
	R2	4.3 ± .7	4.1 ± .9	3.6 ± .8	.0001	.0096
ACA	R1	2.0 ± .0	1.9 ± .3	2.0 ± .0	n.s.	n.s.
	R2	2.0 ± .0	1.9 ± .3	2.0 ± .0	n.s.	n.s.
MCA	R1	3.0 ± .0	2.9 ± .4	2.9 ± .4	n.s.	n.s.
	R2	3.0 ± .0	2.9 ± .4	2.9 ± .4	n.s.	n.s.
PCA	R1	2.0 ± .0	2.0 ± .2	2.0 ± .3	n.s.	n.s.
	R2	2.0 ± .0	2.0 ± .2	2.0 ± .3	n.s.	n.s.
AChA	R1	.2 ± .4	1.2 ± .7	1.3 ± .7	<.0001	n.s.
	R2	.2 ± .4	1.2 ± .7	1.3 ± .7	<.0001	n.s.
SUCA	R1	1.6 ± .6	2.0 ± .2	2.0 ± .2	<.0001	n.s.
	R2	1.6 ± .6	2.0 ± .2	2.0 ± .2	<.0001	n.s.
PCOM left	R1	.5 ± .5	.5 ± .5	.6 ± .5	n.s.	n.s.
	R2	.5 ± .5	.5 ± .5	.6 ± .5	n.s.	n.s.
PCOM right	R1	.4 ± .5	.5 ± .5	.5 ± .5	n.s.	n.s.
	R2	.4 ± .5	.5 ± .5	.5 ± .5	n.s.	n.s.

This table shows the results of the readers' evaluations of large vessel image quality and medium and small vessel detectability according to the scoring system presented in Table 2. Cells provide mean scores ± standard deviation; *P*-values indicate statistical significance for the comparisons of scores (n.s. = not significant considering a level of statistical significance of $P < .05$).
ACA = anterior cerebral artery; AChA = anterior choroidal artery; BA = basilar artery; CS = Compressed SENSE; CTA = CT angiography; ICA = internal carotid artery; MCA = middle cerebral artery; PCA = posterior cerebral artery; PCOM = posterior communicating artery; R1 = reader 1; R2 = reader 2; SUCA = superior cerebellar artery; TOF = time-of-flight; VA = vertebral artery.

agreement for diagnostic confidence was substantial to almost perfect for CTA, TOF-CS, and TOF-Spiral-short imaging data (range of weighted Cohen's kappa: .62-.93).

Diagnostic Performance

All vessel pathologies were correctly identified by both readers in TOF-Spiral-short imaging data compared to the clinical consensus reading without any missed pathology or misclassification of the pathology entity (stenosis, occlusion, or aneurysm).

Quantitative Analysis

Table 4 depicts the results of quantitative assessment of vessel pathology. The maximum diameter of aneurysms showed no significant difference when comparing the measurements obtained in CTA and TOF-CS or TOF-Spiral-short imaging data ($P > .05$), with excellent agreement between the assessments of both readers (range of ICC: .99-1.00). Furthermore, in patients with stenoses, no significant difference was revealed between grading in CTA and TOF-CS or TOF-Spiral-short imaging data ($P > .05$), again obtaining excellent agreement between readers (range of ICC: .94-.99).

Discussion

In this study, we showed that TOF-MRA using spiral imaging can be exploited to generate images of brain-feeding vasculature in a very short time span of only 51 seconds. The TOF-Spiral-short sequence was conceptualized with a slightly smaller FOV than TOF-CS and it exhibited an increased number of artifacts at the skull base. However, it allowed image acquisition with sufficient image quality and high diagnostic confidence when compared to conventional CTA as the gold-standard method and to TOF-MRA accelerated by CS as the hospital-intern reference for TOF-MRA.

Of note, comparing assigned pathologies to the gold-standard assessment of CTA as defined in this study, no false-negative or false-positive classifications were noted, thereby yielding a diagnostic accuracy of 100% in this small patient population. Furthermore, the assessed grade of stenosis and aneurysm diameter according to quantitative measurements showed high accordance among the three imaging modalities, underscoring the high clinical applicability and usability of the images generated by an ultrashort TOF-MRA sequence applying spiral imaging. A high sensitivity and specificity for detection of intracranial pathologies despite small drawbacks in subjective image quality at the skull base might in part be explained by the high accordance in quantitative, non-subjective measurements between imaging using TOF-Spiral-short and TOF-CS. Reliable quantitative measurements are a feature that a radiologist can resort to for a final decision on the assignment of pathologies.

Assessing possible reasons for the critical imaging quality of spiral imaging at the skull base, the most likely explanation is represented by off-resonance effects, which are usually caused by B0 field inhomogeneities that induce blurring when not corrected for. B0 field inhomogeneities are particularly pronounced at air-tissue or bone-tissue interfaces as observed at the skull base, for instance.[31,32] Additionally, some effects of vessel orientation on image quality have been observed for other TOF sequences[33]; hence, such implications might play a role in the context of this study as well. Despite this drawback, spiral imaging seems to offer crucial advantages that could be exploited to

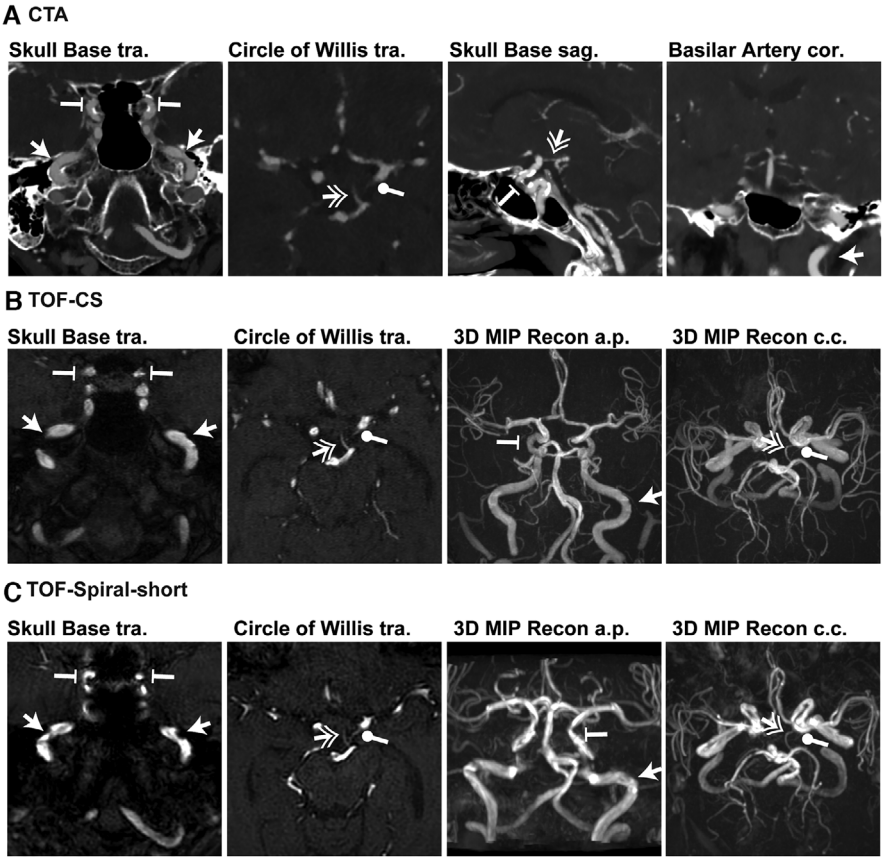

Fig 8. Female patient with vertigo and ataxia undergoing MRI to rule out ischemia of the brain stem. At the junction between extracranial and intraosseous segments of the internal carotid artery (arrows) and between intraosseous and intradural segments of the internal carotid artery (arrows with blunt ends), TOF-Spiral-short shows increased artifacts that reduce image quality. TOF-Spiral-short allows for better depiction of small intracranial vessels like the posterior communicating artery (double arrowhead) and anterior choroidal artery (round arrowhead). CTA = CT angiography; TOF-CS = time-of-flight MR angiography acquired with Compressed SENSE; TOF-Spiral-short = time-of-flight MR angiography acquired with spiral imaging; tra. = transversal; cor. = coronal; sag. = sagittal; MIP = maximum intensity projection; Recon = reconstruction; a.p. = anterior-posterior; c.c. = craniocaudal.

further accelerate image acquisition and to increase the SNR in routine application of TOF-MRA. These consist of scanning with short TEs, thereby limiting the necessity for partial Fourier methods,[34,35] and an intrinsic compensation of higher gradient moments, thereby making imaging less sensitive to flow artifacts,[22,23] which are usually a large caveat in TOF-MRA when blood flow is slow or turbulent.[36] Further potential acceleration could be achieved by 3-dimensional, multislice excitation and parallel imaging.[37,38] Importantly, a 2-dimensional character makes spiral imaging an optimal candidate for undersampling algorithms, as has been achieved in abdominal phase contrast cardiac-gated volume flow measurement by combining it with k-space undersampling via compressed sensing.[39,40]

Possible clinical applications of this ultrashort TOF-MRA sequence are numerous. The intrinsic compensation of higher gradient moments could in part contribute to the observed advantage in delineation of small intracranial vasculature such as the AChA and SUCA. This, in turn, could particularly facilitate imaging of complex vessel pathologies such as arteriovenous malformations or dural arteriovenous fistulas. Increased delineation of small vasculature was observed in a previous publication on spiral-accelerated TOF-MRA at 1.5 Tesla, but was mostly attributed to high spatial resolution.[41] In contrast to that finding, our study showed retention of this benefit even in the setting of an ultrashort sequence with a lower spatial resolution. Furthermore, with only 51 seconds, the acquisition time is much faster compared to the already accelerated TOF-CS and is roughly comparable to standard CTA protocols, with the benefit of absence of radiation exposure and iodinated contrast agents. Despite its decreased FOV and challenging conditions at the skull base regarding diagnostic confidence, pathologies are readily and reliably detected, and their quantification is not inferior to CTA or conventionally used TOF-MRA with CS. With these benefits and radiologists trained to use this sequence for vessel evaluation, TOF-Spiral-short might not only be a good candidate for fast vessel screening purposes but might also augment CTA imaging for stroke diagnostics in selected cases. Specifically, acceleration of TOF-MRA for imaging of brain-feeding arteries is highly important in patients with acute onset neurological deficits, particularly when occurring due to thromboembolic vessel occlusion where reliable but fast imaging is mandatory. Further, short acquisition times also offer benefits when movement artifacts need to be minimized in agitated patients who cannot lie still for a longer time period.

The ultrashort TOF-MRA sequence using spiral imaging was about five times faster than TOF-CS. The improved acquisition time is not completely attributed to the introduction

Table 4. Diagnostic Confidence and Quantitative Assessment of Vessel Pathology

	Reader	CTA	TOF-CS	TOF-Spiral-short	*p* (CTA vs TOF-Spiral-short)	*p* (TOF-CS vs TOF-Spiral-short)
Diagnostic Confidence						
Patients without vessel pathology	R1	2.8 ± .4	2.8 ± .4	2.6 ± .5	n.s.	.0313
(26 patients)	R2	2.6 ± .6	2.8 ± .5	2.4 ± .7	n.s.	.0098
	Kappa	.62	.77	.74	–	–
Patients with vessel pathology	R1	2.6 ± .5	2.5 ± .7	2.4 ± .7	n.s.	n.s.
(15 patients)	R2	2.6 ± .6	2.4 ± .8	2.4 ± .8	n.s.	n.s.
	Kappa	.88	.93	.93	–	–
Quantitative Assessment						
Diameter of aneurysm (in mm,	R1	10.9 ± 10.4	10.7 ± 10.0	10.9 ± 10.4	n.s.	n.s.
evaluated in 5 patients)	R2	10.6 ± 9.9	10.7 ± 10.0	10.5 ± 9.7	n.s.	n.s.
	ICC	.99	1.00	.99	–	–
Degree of stenosis (in %, evaluated	R1	51.3 ± 13.1	52.9 ± 12.5	54.4 ± 10.6	n.s.	n.s.
in 11 patients)	R2	50.5 ± 13.0	51.1 ± 13.1	52.5 ± 11.9	n.s.	n.s.
	ICC	.99	.98	.94	–	–

This table shows the results of the readers' evaluations of diagnostic confidence (separately for patients without and patients with vessel pathology; 1 = low, 2 = intermediate, and 3 = high diagnostic confidence) and quantitative assessments of vessel pathology (maximum diameter of aneurysm, degree of stenosis according to the North American Symptomatic Carotid Endarterectomy Trial [NASCET] criteria). Cells provide mean scores ± standard deviation; *P*-values indicate statistical significance for the comparisons of scores (n.s. = not significant considering a level of statistical significance of $P < .05$). Furthermore, for the assessment of interreader agreement of diagnostic confidence, weighted Cohen's kappa is presented, and interreader correlations for quantitative assessments are depicted by the intraclass correlation coefficient.

CS = Compressed SENSE; CTA = CT angiography; ICC = intraclass correlation coefficient; R1 = reader 1; R2 = reader 2; TOF = time-of-flight.

of spiral imaging. In conservative calculations, we attributed a factor of 1.3 to the acceleration of a given TOF-MRA sequence with spiral imaging. The increase in voxel size constituted a larger increase by a factor of 3.3 compared to TOF-CS, and the reduction in the craniocaudal dimension added an acceleration factor of about 1.2. Nevertheless, increasing the voxel size only is an option if adapted acceleration protocols such as spiral imaging are available. Otherwise, drastic increase in voxel size in conventional TOF-MRA would result in heavy image blurring and decreased precision of interpretation of vessel anatomy. In that regard, the next logical step would be to further exploit spiral imaging by adding undersampling of the k-space through compressed sensing and thus being able to further accelerate a given TOF-MRA sequence protocol. Indeed, taking advantage of k-space undersampling of the high spatial frequencies by using a non-Archimedean spiral trajectory has long been proposed.[42,43] Furthermore, it has already been implemented in blood oxygenation level-dependent functional MRI.[44]

We report no false-negative or false-positive cases, which might appear contradictory to the rather inhomogeneous lumen signal in large vessels at the skull base for imaging by TOF-Spiral-short. However, this issue manifested itself in a decreased rating of vessel quality according to both readers. Furthermore, although all cases were correctly classified as pathologic/non-pathologic, both readers did so with notably decreased diagnostic confidence in TOF-Spiral-short. To support results on detection of vessel pathology in the light of reduced lumen signal quality for TOF-Spiral-short, we additionally performed quantitative assessments of detected vessel pathologies, namely by evaluation of the degree of stenosis. This parameter should be directly linked to vessel signal homogeneity and was found not to be significantly different between CTA, TOF-CS, and TOF-Spiral-short.

This study has several limitations. First, due to the retrospective character of this study and the implementation of TOF-Spiral-short during clinical routine for testing purposes, the routinely used TOF-CS sequence was always acquired first in order, whereas TOF-Spiral-short was acquired directly thereafter. Prospective trials with an alternating or random order of sequences are warranted. Second, the relatively small patient cohort has to be considered a relevant limitation, especially with regard to patients with vessel pathologies as most of the included patients of this study did not present with pathological findings of intracranial vasculature. Third, the small FOV of the TOF-Spiral-short sequence, especially when compared to CTA imaging, excludes assessment of extracranial proximal brain-feeding arteries. Due to the retrospective character of the study, the smaller voxel size and the larger FOV of TOF-CS was not adapted to correlate with the parameters of TOF-Spiral-short. This limits the comparability of both TOF-MRA sequences regarding spatial coverage. Fourth, vessel homogeneity was not independently assessed but included into the qualitative vessel scoring scheme we applied to the extracranial ICA, intraosseous ICA, intradural ICA, VA, and BA. The qualitative assessment of large vessels indeed was able to differentiate between higher quality in CTA and TOF-CS imaging and lower quality for TOF-Spiral-short.

In conclusion, TOF-Spiral-short, an ultrashort TOF-MRA sequence using spiral imaging with an acquisition time of 51 seconds, is considerably faster than routinely acquired TOF-MRA sequences with acceleration by compressed sensing and has not been evaluated in imaging of brain-feeding arteries yet. The TOF-Spiral-short sequence implemented in this study was accelerated through spiral imaging by a factor of approximately 1.3 as well as by slightly reducing the FOV (accelerating the sequence by a factor of 1.2) as well as increasing voxel size (accelerating the sequence by a factor of 3.3). It showed minor drawbacks in image quality of large vessels at the skull base compared to TOF-CS but still may offer sufficient diagnostic performance and confidence in detection and quantitative evaluation of vascular pathologies, if sufficiently resolved by the chosen image resolution. Thus,

this new ultrashort TOF-MRA sequence using spiral imaging may represent a prime alternative in diagnostics of intracranial vessel pathology in the future, most notably in acute stroke diagnostics.

References

1. Writing Group Members, Mozaffarian D, Benjamin EJ, et al. Heart disease and stroke statistics-2016 update: a report from the American Heart Association. Circulation 2016;133: e38-360.
2. Volny O, Kasickova L, Coufalova D, et al. Micrornas in cerebrovascular disease. Adv Exp Med Biol 2015;888:155-95.
3. Hart RG, Diener HC, Coutts SB, et al. Embolic strokes of undetermined source: the case for a new clinical construct. Lancet Neurol 2014;13:429-38.
4. Nussel F, Wegmuller H, Huber P. Comparison of magnetic resonance angiography, magnetic resonance imaging and conventional angiography in cerebral arteriovenous malformation. Neuroradiology 1991;33:56-61.
5. Borisch I, Horn M, Butz B, et al. Preoperative evaluation of carotid artery stenosis: comparison of contrast-enhanced MR angiography and duplex sonography with digital subtraction angiography. AJNR Am J Neuroradiol 2003;24:1117-22.
6. Bui TD, Gelfand D, Whipple S, et al. Comparison of CT and catheter arteriography for evaluation of peripheral arterial disease. Vasc Endovascular Surg 2005;39:481-90.
7. Cirillo M, Scomazzoni F, Cirillo L, et al. Comparison of 3D TOF-MRA and 3D CE-MRA at 3T for imaging of intracranial aneurysms. Eur J Radiol 2013;82:e853-9.
8. Schernthaner R, Stadler A, Lomoschitz F, et al. Multidetector CT angiography in the assessment of peripheral arterial occlusive disease: accuracy in detecting the severity, number, and length of stenoses. Eur Radiol 2008;18:665-71.
9. Wu YW, Leow KS, Zhu Y, et al. Prevention and management of adverse reactions induced by iodinated contrast media. Ann Acad Med Singap 2016;45:157-64.
10. Mandell DM, Mossa-Basha M, Qiao Y, et al. Intracranial vessel wall MRI: principles and expert consensus recommendations of the American Society of Neuroradiology. AJNR Am J Neuroradiol 2017;38:218-29.
11. Chung MS, Jung SC, Kim SO, et al. Intracranial artery stenoocclusion: diagnosis by using two-dimensional spatially selective radiofrequency excitation pulse MR imaging. Radiology 2017;284:834-43.
12. Lee NJ, Chung MS, Jung SC, et al. Comparison of high-resolution MR imaging and digital subtraction angiography for the characterization and diagnosis of intracranial artery disease. AJNR Am J Neuroradiol 2016;37:2245-50.
13. Park JE, Jung SC, Lee SH, et al. Comparison of 3D magnetic resonance imaging and digital subtraction angiography for intracranial artery stenosis. Eur Radiol 2017;27:4737-46.
14. Patel MR, Klufas RA, Kim D, et al. MR angiography of the carotid bifurcation: artifacts and limitations. AJR Am J Roentgenol 1994;162:1431-7.
15. Fushimi Y, Fujimoto K, Okada T, et al. Compressed sensing 3-dimensional time-of-flight magnetic resonance angiography for cerebral aneurysms: optimization and evaluation. Invest Radiol 2016;51:228-35.
16. Lustig M, Donoho D, Pauly JM. Sparse MRI: the application of compressed sensing for rapid MR imaging. Magn Reson Med 2007;58:1182-95.
17. Yamamoto T, Okada T, Fushimi Y, et al. Magnetic resonance angiography with compressed sensing: an evaluation of moyamoya disease. PLoS One 2018;13:e0189493.
18. Lu SS, Qi M, Zhang X, et al. Clinical evaluation of highly accelerated compressed sensing time-of-flight MR angiography for intracranial arterial stenosis. AJNR Am J Neuroradiol 2018;39: 1833-8.
19. Li B, Li H, Dong L, et al. Fast carotid artery MR angiography with compressed sensing based three-dimensional time-of-flight sequence. Magn Reson Imaging 2017;43:129-35.
20. Fushimi Y, Okada T, Kikuchi T, et al. Clinical evaluation of time-of-flight MR angiography with sparse undersampling and iterative reconstruction for cerebral aneurysms. NMR Biomed 2017;30:e3774.
21. Hutter J, Grimm R, Forman C, et al. Highly undersampled peripheral time-of-flight magnetic resonance angiography: optimized data acquisition and iterative image reconstruction. MAGMA 2015;28:437-46.
22. Meyer CH, Hu BS, Nishimura DG, et al. Fast spiral coronary artery imaging. Magn Reson Med 1992;28:202-13.
23. Amann M, Bock M, Floemer F, et al. Three-dimensional spiral MR imaging: application to renal multiphase contrast-enhanced angiography. Magn Reson Med 2002;48:290-6.
24. Wang D, Zwart NR, Pipe JG. Joint water-fat separation and deblurring for spiral imaging. Magn Reson Med 2018;79:3218-28.
25. Li Z, Hu HH, Miller JH, et al. A spiral spin-echo MR imaging technique for improved flow artifact suppression in T1-weighted postcontrast brain imaging: a comparison with Cartesian turbo spin-echo. AJNR Am J Neuroradiol 2016;37:642-7.
26. Greve T, Sollmann N, Hock A, et al. Highly accelerated time-of-flight magnetic resonance angiography using spiral imaging improves conspicuity of intracranial arterial branches while reducing scan time. Eur Radiol 2020;30:855-65.
27. Sollmann N, Mei K, Riederer I, et al. Tube current reduction in CT angiography: how low can we go in imaging of patients with suspected acute stroke? AJR Am J Roentgenol 2019;213: 410-6.
28. Samuels OB, Joseph GJ, Lynn MJ, et al. A standardized method for measuring intracranial arterial stenosis. AJNR Am J Neuroradiol 2000;21:643-6.
29. Fox AJ. How to measure carotid stenosis. Radiology 1993;186: 316-8.
30. Bash S, Villablanca JP, Jahan R, et al. Intracranial vascular stenosis and occlusive disease: evaluation with CT angiography, MR angiography, and digital subtraction angiography. AJNR Am J Neuroradiol 2005;26:1012-21.
31. Block KT, Frahm J. Spiral imaging: a critical appraisal. J Magn Reson Imaging 2005;21:657-68.
32. Bornert P, Schomberg H, Aldefeld B, et al. Improvements in spiral MR imaging. MAGMA 1999;9:29-41.
33. Morelli JN, Gerdes CM, Schmitt P, et al. Technical considerations in MR angiography: an image-based guide. J Magn Reson Imaging 2013;37:1326-41.
34. Kasper L, Haeberlin M, Dietrich BE, et al. Matched-filter acquisition for bold fMRI. Neuroimage 2014;100:145-60.
35. Ahn CB, Kim JH, Cho ZH. High-speed spiral-scan echo planar NMR imaging-I. IEEE Trans Med Imaging 1986;5:2-7.
36. Kaufmann TJ, Huston J 3rd, Cloft HJ, et al. A prospective trial of 3T and 1.5T time-of-flight and contrast-enhanced MR angiography in the follow-up of coiled intracranial aneurysms. AJNR Am J Neuroradiol 2010;31:912-8.
37. Zahneisen B, Poser BA, Ernst T, et al. Simultaneous multi-slice fMRI using spiral trajectories. Neuroimage 2014;92:8-18.
38. Heberlein K, Hu X. Auto-calibrated parallel spiral imaging. Magn Reson Med 2006;55:619-25.
39. Dyvorne H, Knight-Greenfield A, Jajamovich G, et al. Abdominal 4D flow MR imaging in a breath hold: combination of spiral sampling and dynamic compressed sensing for highly accelerated acquisition. Radiology 2015;275:245-54.
40. Bane O, Peti S, Wagner M, et al. Hemodynamic measurements with an abdominal 4D flow MRI sequence with spiral sampling and compressed sensing in patients with chronic liver disease. J Magn Reson Imaging 2019;49:994-1005.
41. Sartoretti T, van Smoorenburg L, Sartoretti E, et al. Ultrafast intracranial vessel imaging with non-Cartesian spiral 3-dimensional time-of-flight magnetic resonance angiography at 1.5 T: an

in vitro and clinical study in healthy volunteers. Invest Radiol 2020;55:293-303.
42. Tsai CM, Nishimura DG. Reduced aliasing artifacts using variable-density k-space sampling trajectories. Magn Reson Med 2000;43:452-8.
43. Kim DH, Adalsteinsson E, Spielman DM. Simple analytic variable density spiral design. Magn Reson Med 2003;50: 214-9.
44. Glover GH. Spiral imaging in fMRI. Neuroimage 2012;62: 706-12.